Available online at www.sciencedirect.com

ScienceDirect

Procedia IUTAM 14 (2015) 519 – 526

Procedia IUTAM

www.elsevier.com/locate/procedia

IUTAM_ABCM Symposium on Laminar Turbulent Transition

Transition to turbulence in viscoelastic channel flow

Akshat Agarwal[a], Luca Brandt[b], Tamer A. Zaki[a,*]

[a]*Department of Mechanical Engineering, Imperial College London, London SW7 2AZ, UK*
[b]*Linné Flow Centre, SeRC, KTH Mechanics, Stockholm, SE-100 44, Sweden*

Abstract

The influence of viscoelasticity on bypass transition to turbulence in channel flow is studied using data from direct numerical simulations by Agarwal et al. (2014)[1]. The initial field is a superposition of a laminar base state and a localized disturbance. Relative to the Newtonian conditions, the polymeric FENE-P flow delays the onset of transition and extends its duration. The former effect is due to a weakening of the pre-transitional disturbance field, while the prolonged transition region is due to a slower spreading rate of the turbulent spots. Once turbulence occupies the full channel, a comparison of the turbulence fields shows that energetic flow structures are longer and wider in the polymeric flow. The final turbulent state is compared to elasto-inertial turbulence (EIT), where the polymer conformation field takes the form of elongated sheets with wide spanwise extent.

Selection and peer-review under responsibility of ABCM (Brazilian Society of Mechanical Sciences and Engineering)

1. Introduction

The process of bypass transition triggered by a localized disturbance in channel flow[2] can be divided into three successive stages. The first is linear growth and is characterized by an amplification of the disturbance energy due to the lift-up mechanism. This is followed by non-linear growth where streaky structures become dominant. These structures are made up of high streamwise velocity fluctuations. The streaks eventually break down due to a secondary instability mechanism[3,4] which takes the form of a roll-up process, leading to the creation of a turbulent spot and the onset of turbulence. While turbulence ultimately fills the channel in both the Newtonian and polymeric flow, the final flow states are remarkably different: Drag can be significantly reduced in the polymer flow relative to the Newtonian case[5,6,7,8].

The drag reducing effect of polymers in fully turbulent wall-bounded flows was discovered by Toms (1948)[5] and, due to its practical applications, has been the subject of several studies since. Direct Numerical Simulations (DNS) have been employed extensively to understand this phenomenon. These efforts have shed light on the effects of polymers on the turbulent kinetic energy statistics[9,10] and on the flow structures through calculations in minimal flow units[11,8]. Drag reduction in fully turbulent channel flow has been reported to increase with increasing elasticity of the flow. An upper limit of this phenomenon, referred to as maximum drag reduction (MDR), has been documented[12] and is characterized by a mean velocity profile called the Virk asymptote. In recent studies[13,14], the state of elasto-

* Corresponding author. Tel.: +44-20-7594-7032.
E-mail address: t.zaki@imperial.ac.uk

Selection and peer-review under responsibility of ABCM (Brazilian Society of Mechanical Sciences and Engineering)
doi:10.1016/j.piutam.2015.03.083

inertial turbulence has been proposed as an explanation for the maximum drag reduction limit. Flow structures which characterize this state consist of alternating spanwise oriented regions of rotational and extensional flow[14]. The authors propose that the polymers are stretched in laminar flow by the action of shear. Upon the introduction of disturbance in the flow, regions of high polymer extension arranged in the form of thin sheets are formed, which are tilted upwards in the wall-normal direction. The large extension of the polymer sheets results in an increase of the extensional viscosity of the flow in this region.

In the current study, we analyze results from the first direct numerical simulations of bypass transition in polymeric channel flow[1]. The simulations capture the evolution of a three dimensional localized disturbance in non-Newtonian channel flow through the transition process and up to the resulting drag-reduced turbulent state. The FENE-P model is adopted to simulate a dilute polymeric solution, and the parameters of the simulations are designed to lead to an MDR state.

2. Setup

For a polymeric solution of uniform concentration, the governing flow equations are,

$$\partial_t u_i + u_j \partial_j u_i = -\partial_i p + \frac{\beta}{Re}\partial_j \partial_j u_i + \frac{1-\beta}{Re}\partial_j \tau_{ij}; \quad \partial_j u_j = 0 \tag{1}$$

$$\partial_t c_{ij} + u_k \partial_k c_{ij} = c_{kj}\partial_k u_i + c_{ik}\partial_k u_j - \tau_{ij}. \tag{2}$$

$$\tau_{ij} = \frac{1}{We}\left(\frac{c_{ij}}{1 - c_{kk}/L^2_{max}} - \frac{\delta_{ij}}{1 - 3/L^2_{max}}\right). \tag{3}$$

In the equations above, β is the ratio of the solvent viscosity to the total viscosity and τ_{ij} is the stress tensor representing the interaction between the polymer chain and the solvent. The conformation of the polymer chains is given by the tensor c_{ij}. The Weissenberg number, We, is the ratio of the polymer relaxation time to the flow time scale, and the extensibility of the polymer chain is limited to a maximum prescribed value, L_{max}. Instantaneous flow variables are decomposed according to $\phi(\mathbf{x}, t) = \overline{\phi}(y, t) + \phi'(\mathbf{x}, t)$, where $\overline{\phi}(y, t)$ is the streamwise and spanwise average and $\phi'(\mathbf{x}, t)$ is the perturbation.

The localized disturbance which triggers transition is a pair of counter-rotating vortices aligned in the streamwise direction (see figure 1), and was previously used in the Newtonian literature[2]. The disturbance streamfunction and velocity are,

$$\psi = \epsilon f(y)\left(\frac{x'}{l_x}\right) z' exp\left[-\left(\frac{x'}{l_x}\right)^2 - \left(\frac{z'}{l_z}\right)^2\right] \tag{4}$$

$$(u', v', w') = \left(-\frac{\partial \psi}{\partial y} sin\theta, \frac{\partial \psi}{\partial z'}, -\frac{\partial \psi}{\partial y} cos\theta\right) \tag{5}$$

$$(x', z') = (xcos\theta - zsin\theta, xsin\theta + zcos\theta) \tag{6}$$

$$f(y) = (1 + y)^p (1 - y)^q. \tag{7}$$

The constants l_x, l_y and l_z are the streamwise, wall-normal and spanwise length scales of the disturbance and ϵ is its amplitude. For this study, $l_x = l_z = 2$. The exponents of the wall-normal dependence are also equal, $p = q = 2$.

This disturbance is added to a non-Newtonian laminar base flow in the channel and simulations are performed at Reynolds number $Re = 2{,}000$ based on the channel half height and bulk flow velocity in a constant mass flow rate configuration. A grid refinement study was carried out in order to ensure that the flow is fully resolved.

The computational domain for all simulations presented herein has dimensions $L_x = 48$, $L_y = 2$, $L_z = 24$ in the streamwise, wall-normal and spanwise directions respectively. The spatial discretization of the Navier-Stokes equations is performed using a control-volume formulation. The equations are advanced in time using a fractional-step algorithm where the diffusion and polymer stress terms are treated implicitly using Crank-Nicholson, and the advection terms are treated explicitly. Spatial derivatives of the conformation tensor in equation 2 are computed using a third order upwind central scheme. To ensure numerical stability, a local artificial diffusivity is added at locations where the conformation tensor loses its positive definiteness[15]. Artificial diffusivity is restricted to less than 10 % of the grid nodes, which is consistent with previous studies[16].

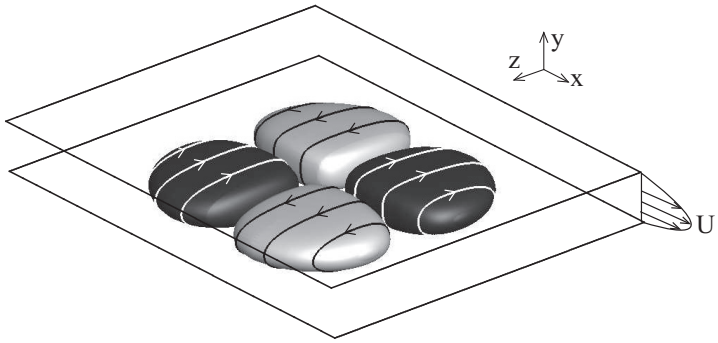

Fig. 1. The localized disturbance represented by iso-surfaces of the streamwise vorticity. The grey surface represents positive vorticity and the dark surface, negative vorticity. The iso-surfaces are marked with streamtraces of the perturbation velocity.

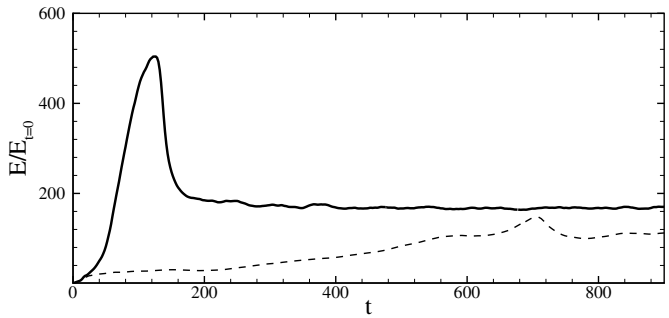

Fig. 2. Energy amplification for the large amplitude vortex pair. ——: Newtonian; – – –: $We = 15, \beta = 0.9, L_{max} = 100$.

3. Results

The overall effect of the polymer is a delay in transition to turbulence and reaching a statistically stationary turbulent state. For the results presented, $We = 15$, $\beta = 0.9$ and $L_{max} = 100$. The transition process is prolonged, as shown by the evolution of the total perturbation energy plotted in figure 2. The friction Reynolds numbers achieved in the fully-turbulent state are $Re_\tau = 132$ for the Newtonian case and $Re_\tau = 90$ for the polymer flow. Figure 2 shows that the suppression of disturbance energy begins in the linear growth phase. During this early time, the spanwise and wall-normal components of the polymer contribution to the perturbation energy budget (polymer work) are negative ($t = 0$ to $t = 10$ in figure 3). This results in a supression of the corresponding spanwise and wall-normal velocity perturbations, leading to a lower rate of energy growth.

Further evolution of the disturbance leads to the formation of streaky structures which become dominant, and mark the beginning of the non-linear growth phase. The formation of these structures is resisted by the negative streamwise component of polymer work, as seen beyond $t = 15$ in figure 3. The structures with high streamwise perturbation velocity are therefore weaker in non-Newtonian flow than in Newtonian flow, which is in agreement with the observations from calculations in minimal flow units[8]. Another point of difference in non-Newtonian flow which results in the prolonged transition process is the slower pace at which turbulence spreads across the channel. The

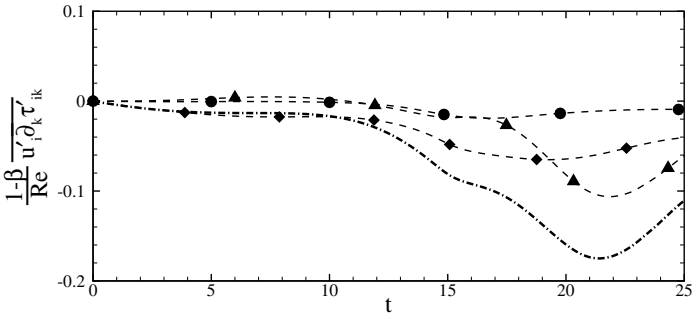

Fig. 3. Components of polymer work during the early stages of transition. – · – · –: Total polymer work; ▲: streamwise; ♦: spanwise; •: wall-normal.

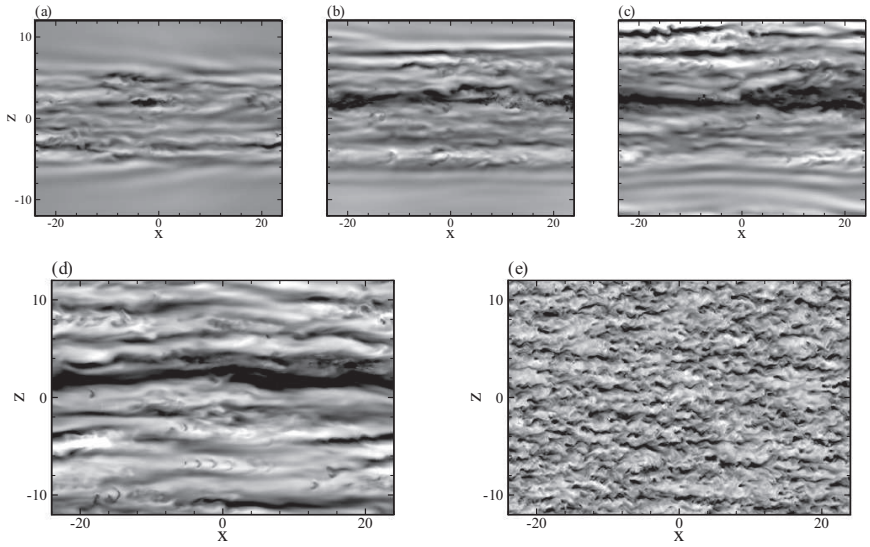

Fig. 4. Snapshots of u' at $y = -0.56$ during the evolution of the large amplitude vortex pair. Figures (a) to (c) represent non-Newtonian flow during transition at We= 15, $L_{max} = 100$, $\beta = 0.9$ and $t = \{200, 400, 600\}$. (d) and (e) are a comparison of non-Newtonian and Newtonian flows, respectively, at $t = 900$. Contour limits: [−0.2 0.2].

snapshots in figure 4a-c show this spreading process, which spans approximately 750 time units relative to 200 time units in the Newtonian case.

Even when turbulence occupies the entire channel, the Newtonian and polymeric flow still differ substantially. Comparison of instantaneous perturbation fields (see figures 4*d* and *e*) shows that the turbulence structures have a larger extent in both the streamwise and spanwise directions in the non-Newtonian case. For a quantitative assessment of this difference, the energy spectral density for the turbulent regime in both flow configurations is plotted in figure 5.

The energy distribution across the wavenumbers confirms the observations from the snapshots in figure 4. In the streamwise direction (figure 5a), in Newtonian flow, energy is highest at the smaller wavenumbers, with a decrease in energy for higher values of k_x. This effect is amplified in non-Newtonian flow (figure 5b). The magnitude of energy for small k_x is larger than in Newtonian flow. This is followed by a steep drop-off in energy for higher wavenumbers, which indicates that the energy is concentrated at very low streamwise wavenumbers. In the spanwise direction, energy across the wavenumber spectrum in Newtonian flow is distributed more evenly than in the streamwise direction with

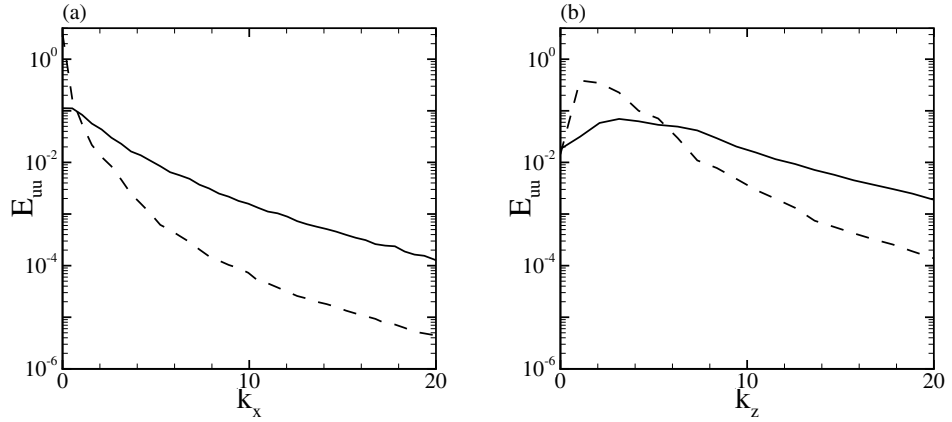

Fig. 5. Energy spectra of u' at $Re_b = 2000$ and $y = -0.56$ in turbulent flow. (a) Streamwise, (b) spanwise. ——: Newtonian flow, – – –: non-Newtonian flow at We= 15, $L_{max} = 100, \beta = 0.9$.

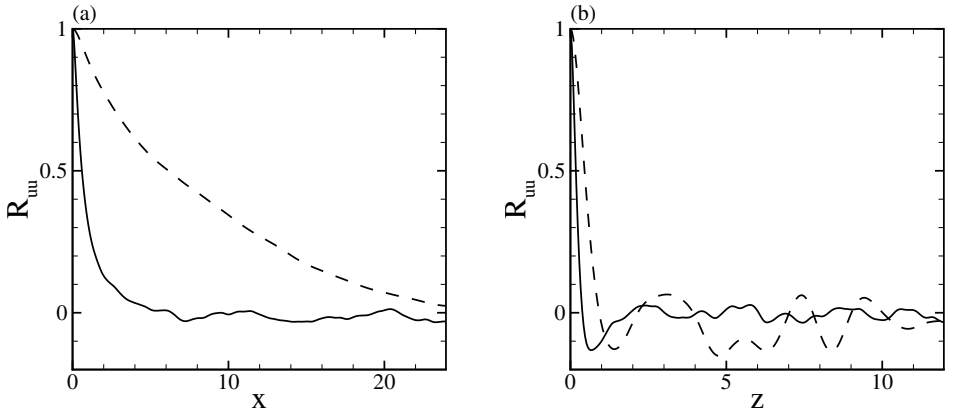

Fig. 6. Two point correlation of u' at $Re_b = 2000$ and $y = -0.56$ in turbulent flow. (a) Streamwise separation, (b) spanwise separation. ——: Newtonian flow, – – –: non-Newtonian flow at We= 15, $L_{max} = 100, \beta = 0.9$.

a peak at $k_z \sim 2$. In non-Newtonian flow, the magnitude of energy in the lower wavenumber regime is considerably higher and the peak moves to a smaller wavenumber.

The differences in the energy spectrum between Newtonian and non-Newtonian flow point to differences in flow structures in the two configurations. The two-point correlations of the streamwise velocity perturbation in the streamwise and spanwise directions are plotted in figure 6. There is a considerable difference in the correlation in the streamwise direction. In Newtonian flow, the correlation drops to a negligible value beyond $x \sim 5$, indicating that the extent of the largest streamwise structure is only a fraction of the domain. In non-Newtonian flow, the correlation is higher across the channel but reaches a minima at $x = L_x/2$. Simulations of fully turbulent viscoelastic flow have previously been performed for a range of domain sizes in regimes of varying drag reduction [17]. For the maximum drag reduction scenario, the current result for streamwise correlation in figure 6 is in agreement with the published results for a computational domain with a comparable streamwise extent. The higher correlation in the non-Newtonian configuration indicates the presence of flow structures which are considerably longer in the streamwise direction. This supports the empirical observations from figure 4*d* and *e*.

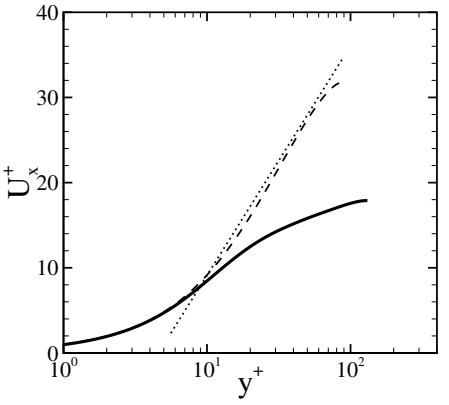

Fig. 7. Mean velocity profiles normalized using inner variables. ——: Newtonian; – – –: $We = 15, \beta = 0.9, L_{max} = 100$; · · · · · ·: Virk asymptote.

The difference in the two-point correlation between Newtonian and non-Newtonian flow in the spanwise direction is clearly visible in figure 6*b*. The first minima of the correlation is an indication of the spanwise size of the dominant flow structures. In Newtonian flow, this minima occurs at $z \sim 0.7$, while in non-Newtonian flow, the width $z \sim 1.5$, indicative of wider structures. This supports qualitative comparisons of the spanwise extent of the flow structures from snapshots of the flow (figure 4d and e).

For this study, the turbulent viscoelastic flow is in a Maximum Drag Reduction (MDR) state. This is confirmed by the mean velocity profile in figure 7 which matches the Virk Asymptote. In recent literature on viscoelastic channel flow, an MDR state at moderate Reynolds number has been described as "elasto-inertial turbulence" (EIT)[13,14]. The mean flow profile for the current study (figure 7) matches that description. Samanta et al. (2013) also note that EIT is characterized by sheet-like structures of polymer extension which are large in the streamwise and spanwise dimensions, which warrants a comparison to the structures observed in the current simulations.

In the work by Samanta et al. (2013), the spanwise extent of each structure of polymer extension is as large as their computational domain and the streamwise extent is a considerable portion of the channel. In addition, the flow alternately goes through an active state in which the structures are strong and a hibernating state in which they weaken. Large structures of polymer extension with a physical size similar to those reported for EIT[13] are also established in the fully turbulent state of the current study (figure 8). The ratio of the polymeric extension to maximum extensibility plotted along the vertical walls in the figure shows that the sheet-like structures are tilted at an upward angle from the streamwise direction, as reported for EIT. The pressure perturbations which redistribute energy across components of momentum in response to the polymer stretching[14], are plotted along the bottom wall. Though there are similarities in the plotted structures of polymer extension and pressure perturbation with EIT, they do not exhibit the near spanwise independence of the structures in that regime. Our computational domain is, however, five times larger in each of the horizontal dimensions. As a result, the structures occupy only a fraction of the channel.

In a subset of the current domain, comparable in size to that in studies of EIT, the plotted variables appear very similar to those reported (compare figure 8b with figure 4b of Samanta et al. (2013)[13]). The sheets of polymer extension as well as the pressure perturbations cover a considerable part of this subdomain. This two-dimensional nature of the structures is replicated intermittently in the large domain.

4. Conclusions

The current study reports on the first direction numerical simulations of bypass transition to turbulence in viscoelastic channel flow. Elasticity has a dual effect in the transition regime: It weakens the amplification of the pre-transitional disturbance field and as a result delays the onset of transition. It also reduces the spreading rate of the turbulence spots and hence prolongs the transition period. Beyond transition, the polymeric flow reaches a fully-turbulent MDR state. A comparison of the energy spectral density with the Newtonian flow reveals that more energy is concentrated in

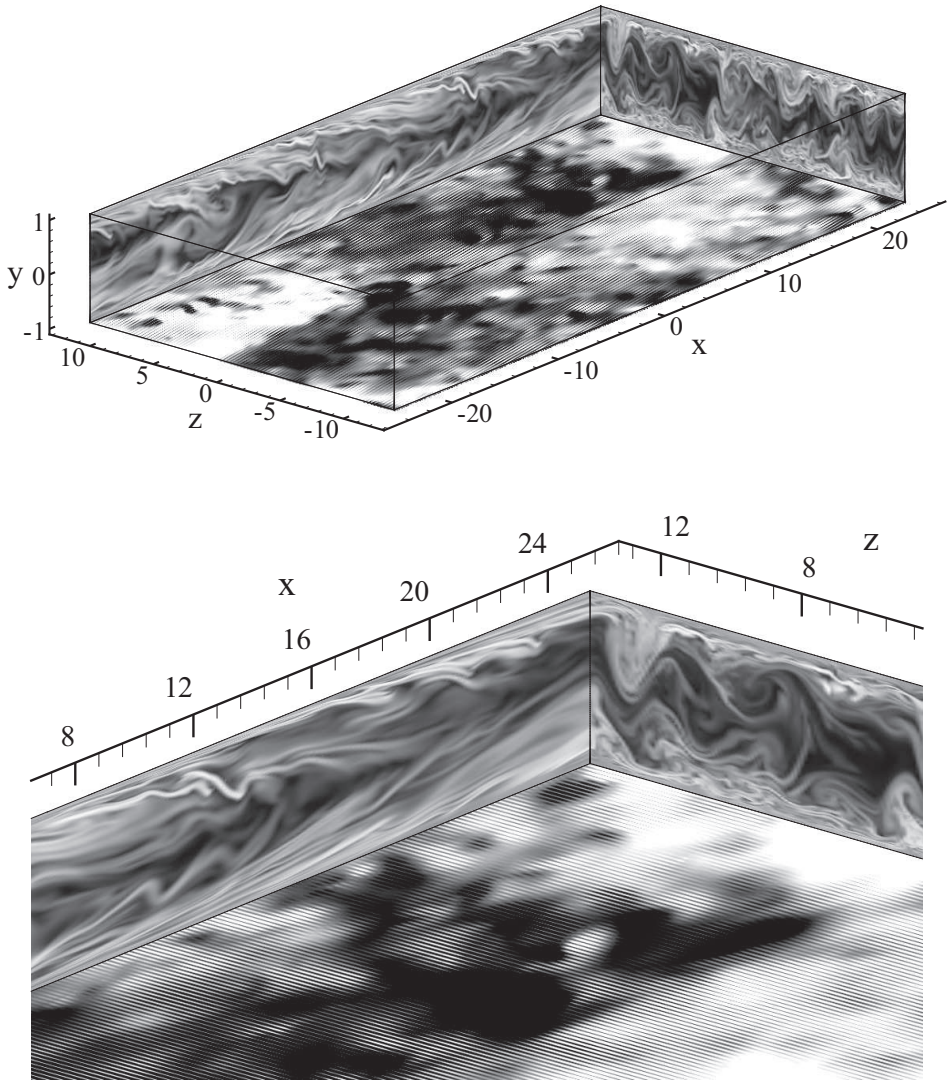

Fig. 8. Top: snapshot of fully turbulent flow at $Re = 2{,}000$, $We = 15$, $L_{max} = 100, \beta = 0.9$. Contours along the vertical walls represent $\sqrt{tr(C)}/L_{max}$ with limits [0 0.9]. Along the horizontal wall, p' is plotted with limits [−0.004 0.004]. Bottom: a zoomed-in view of the top figure.

the lower horizontal wavenumbers in the presence of elasticity. This is supported by the two point correlations of u', which indicate the presence of larger flow structures in both the streamwise and spanwise directions. Relative to previous studies, our simulation parameters fall in the regime of elasto-inertial turbulence. The literature on EIT indicates that the polymer conformation field takes the form of two-dimensional structures that have the same width as the channel. Our simulations adopted a computational domain that is much larger in the horizontal dimensions than previous studies. Our results demonstrate that these structures are not two dimensional, but rather very wide in the spanwise direction.

References

1. A. Agarwal, L. Brandt, T. A. Zaki, Linear and non-linear evolution of a localized disturbance in polymeric channel flow, Journal of Fluid Mechanics (2014) Accepted.
2. D. S. Henningson, A. Lundbladh, A. V. Johansson, A mechanism for bypass transition from localized disturbances in wall-bounded shear flows, Journal of Fluid Mechanics 250 (1993) 169–207.
3. N. J. Vaughan, T. A. Zaki, Stability of zero-pressure-gradient boundary layer distorted by unsteady klebanoff streaks, Journal of Fluid Mechanics 681 (2011) 116–153.
4. M. J. P. Hack, T. A. Zaki, Streak instabilities in boundary layers beneath free-stream turbulence, Journal of Fluid Mechanics 741 (2014) 280–315.
5. B. Toms, Observation on the flow of linear polymer solutions through straight tubes at large Reynolds numbers, Proceedings of the International Rheological Congress 2 (1948) 135–141.
6. J. L. Lumley, Drag reduction by additives, Annual Review of Fluid Mechanics 1 (1969) 367–384.
7. C. M. White, M. G. Mungal, Mechanics and prediction of turbulent drag reduction with polymer additives, Annual Review of Fluid Mechanics 40 (2008) 235–256.
8. L. Xi, M. D. Graham, Turbulent drag reduction and multistage transitions in viscoelastic minimal flow units, Journal of Fluid Mechanics 647 (2010) 421–452.
9. R. Sureshkumar, A. N. Beris, R. A. Handler, Direct numerical simulation of the turbulent channel flow of a polymer solution, Physics of Fluids 9 (1997) 743–755.
10. V. Dallas, J. C. Vassilicos, G. F. Hewitt, Strong polymer-turbulence interactions in viscoelastic turbulent channel flow, Physical Review E 82 (2010) 066303.
11. P. A. Stone, W. Waleffe, M. D. Graham, Toward a structural understanding of turbulent drag reduction: nonlinear coherent states in viscoelastic shear flows, Phys. Rev. Lett. 89 (2002) 208301.
12. P. S. Virk, H. S. Mickley, The ultimate asymptote and mean flow structures in Tom's phenomenon, Trans. ASME E: J. Appl. Mech. 37 (1970) 488–493.
13. D. Samanta, Y. Dubief, M. Holzner, C. Schafer, A. N. Morozov, Elasto-inertial turbulence, PNAS 110 (2013) 10557–10562.
14. Y. Dubief, V. E. Terrapon, J. Soria, On the mechanism of elasto-inertial turbulence, Physics of Fluids 25 (2013) 110817.
15. T. Min, J. Y. Yoo, H. Choi, Effect of spatial discretization schemes on numerical solutions of viscoelastic fluid flows, Journal of Non-Newtonian Fluid Mechanics 100 (2001) 27–47.
16. Y. Dubief, V. E. Terrapon, C. M. White, E. S. G. Shaqfeh, P. Moin, S. K. Lele, New answers on the interaction between polymers and vortices in turbulent flows, Flow, Turbulence and Combustion 74 (2005) 311–329.
17. C.-F. Li, R. Sureshkumar, B. Khomami, Influence of rheological parameters on polymer induced turbulent drag reduction, Journal of Non-Newtonian Fluid Mechanics 140 (2006) 23–40.